Efimov effect of triple-stranded DNA: Real-space renormalization group and zeros of the partition function

Jaya Maji[*] and Somendra M. Bhattacharjee[†]

Institute of Physics, Bhubaneswar-751005, India
(Received 17 July 2012; published 25 October 2012)

We study the melting of three-stranded DNA by using the real-space renormalization group and exact recursion relations. The prediction of an unusual Efimov-analog three-chain bound state, that appears at the critical melting of two-chain DNA, is corroborated by the zeros of the partition function. The distribution of the zeros has been studied in detail for various situations. We show that the Efimov DNA can occur even if the three-chain (i.e., three-monomer) interaction is repulsive in nature. In higher dimensions, a striking result that emerged in this repulsive zone is a continuous transition from the critical state to the Efimov DNA.

I. INTRODUCTION

In recent times the formation of triple-helical DNA has been a topic of considerable importance because of possible implications in the field of molecular biology. In 1957, it was discovered that certain sequences of Watson-Crick double-helical DNA allow a third strand of DNA to bind via Hoogsteen or reverse Hoogsteen base pairing to form a triple helix [1–3]. This triple-helix formation has the potentiality to block transcription and thereby affect gene expression. Following this discovery, the experimental demonstration of the ability of a third chain to recognize the base sequences without the double-helical DNA revealing the base pairs renewed the interest in triple-helix DNA, especially its therapeutic applications [4,5]. It is now known that not only DNA but even RNA [6] and PNA (polypeptide nucleic acid) are capable of forming a triple helix with duplex DNA [7,8].

Three-stranded DNA has been shown to exhibit an Efimov-like bound state near or at the critical melting of duplex DNA [9]. The Efimov effect is the most striking phenomenon to occur in quantum three-body systems with only two-body short-range pair interactions [10–13]. An infinite number of bound states appear at the critical threshold of two-body binding. There are several theoretical and experimental investigations using different models and methods that show this effect [14–17]. The universality of this phenomenon encompasses the analogous classical model, namely, the melting of three-stranded DNA [9]. An analogy is drawn between the large quantum fluctuations near the zero-energy threshold of two-body binding and the thermal Gaussian fluctuations at the melting of duplex DNA. As discussed in Ref. [9], there is an exact mapping of the partition function of three ideal polymers with DNA base-pairing-type short-range interaction to the Green function of three-particle quantum mechanics under a transformation of the length of polymers to imaginary time. Furthermore, a scaling argument was used there to justify the occurrence of the effective two-chain attractive potential $\frac{1}{r^2}$ as a source of the Efimov effect. Such a long-range interaction leads to a broad three-strand DNA bound state at or beyond the melting point of duplex DNA. This is a state where no two

strands are bound but the three are bound together. We called this loosely bound state Efimov DNA [18]. This has also been observed from the renormalization group (RG) flows and exact numerical calculations for several model systems, in particular on hierarchical lattices.

Hierarchical lattices, by virtue of their discrete scaling, allow one to solve many models in statistical mechanics by exact renormalization group transformations [19–22]. Furthermore, many approximate real-space RGs on real lattices can be viewed as exact real-space RGs on hierarchical lattices. In the first study of the Efimov effect for Gaussian polymers, RG and exact numerics were used [9]. A part of our aim here is to analyze the Efimov phenomena exhibited by triple-stranded DNA from the classical phase transition point of view, especially by looking at the zeros of the partition functions.

Finding the zeros of a partition function in the complex plane of any physical variable is a mathematical way to understand and analyze phase transition phenomena. However, finding those is often possible only for small sizes or soluble cases and not in general. Yang and Lee first studied the Ising ferromagnetic system in a complex magnetic field to show that for a properly chosen variable the zeros lie on a unit circle, known as the Yang-Lee circle [23,24]. Later the zeros were studied in the complex temperature plane and other variables [25]. Since there cannot be any real zero, the zeros may accumulate and pinch the real axis at a limit point in the thermodynamic limit. This limit point then identifies a transition point. This method can provide relevant information on phase transitions such as the critical field or temperature and the values of the associated critical exponents. Moreover, the distribution of zeros may form many complicated structures other than a circle. These structures are the separatrices of the two types of flow to the two different stable fixed points of the RG transformation, and are similar to the Julia sets (see Appendix B) [26,27].

In Ref. [9] the RG flows were studied in the unbound region of the two- and the three-chain states. By looking at the flows in the unbound region of duplex DNA, where the chains are supposed to be free, an effective three-chain bound state was predicted. In this paper we study the partition function of the three-chain system by combining the recursion relations and the RG transformations, and then finding the zeros. We also extend the model to the three-chain repulsive interaction regime. In addition, we discuss several other features of the

---

[*]jayamaji@iopb.res.in

[†]somen@iopb.res.in

zeros in the complex plane, for instance the detailed structure, and the connection to the Julia set.

This paper is organized as follows. In Sec. II, the three-polymer problem on a hierarchical lattice is introduced. In Sec. III, the recursion relations from RG decimation and those for exact iterations are written. The method of finding the zeros of the partition function is discussed, and we find the limit point of the zeros to locate the phase transition. Section IV contains the results and discussions on the two- and the three-chain systems under different situations. In particular we estimate the transition point for Efimov DNA. Section V extends the problem to three-chain repulsive interactions. The existence of a transition between the Efimov DNA and the critical repulsive state in higher dimensions is established there. Appendices B and C describe the Julia set and the limit cycle.

II. MODEL

Let us consider the diamond hierarchical lattice as shown in Fig. 1. The lattice is generated iteratively by the replacement of each bond at the $(n-1)$th generation by a motif of λb bonds to get the nth generation, where λ and b represent the bond scaling factor and the branching factor, respectively. The thermodynamic limit is obtained as $n \to \infty$ and in that limit the effective dimensionality of the lattice is

$$d = \frac{\ln \lambda b}{\ln \lambda}. \tag{1}$$

In this paper we shall choose $\lambda = 2$.

One major feature about hierarchical lattices is their unusual scale invariance property. They have a discrete scaling symmetry. That is why an exact implementation of the real-space RG technique is possible. The decimation of the nth generation to arrive at the $(n-1)$th generation is precisely what is needed in a RG transformation. Once the partition function is known, it is possible to calculate the free energy and the other thermodynamic quantities. One may even write down recursion relations for them.

We consider three directed polymers on a diamond hierarchical lattice. Three chains on the diamond hierarchical lattice are stretched from bottom to top, but they can wander at intermediate points. The contact energies are defined at the bonds only. The polymers are assigned attractive potentials $-\epsilon$ and $-\epsilon_{123}$ ($\epsilon, \epsilon_{123} > 0$) if a single bond is shared by two and three polymers, respectively (see Fig. 2). At each generation, the length of each polymer increases by a factor $\lambda = 2$ so that the length of polymers at the nth generation is
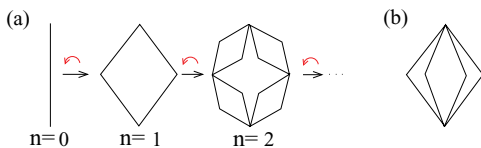
$$L_n = 2^n. \tag{2}$$

FIG. 1. (Color online) (a) The recursive construction of the hierarchical lattice with $b = 2$ for $n = 0, 1, 2, \ldots$ generations. The right arrows represent the direction of iteration towards larger lattices. The left arrows represent the direction of decimation used in the RG. (b) A motif of $2b$ bonds, where $b = 4$.
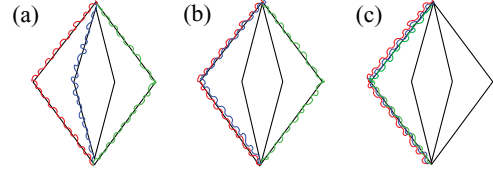

FIG. 2. (Color online) Examples of three-chain configurations on a diamond motif for $b = 4$. (a) The polymers do not share any single bond. The number of such configurations is $b(b-1)(b-2)$. (b) Two polymers share a bond. The energy here is -2ϵ and the number of such configurations is $b(b-1)$. (c) Three polymers share the same bond. The energy is $2(-3\epsilon - \epsilon_{123})$. The number of such configurations is b.

For the Efimov effect, just pairwise interaction is enough. However, in a RG procedure it is imperative to define the model with both ϵ and ϵ_{123}, because the three-chain interaction gets generated on a longer scale.

III. METHOD

A. Renormalization group

In this section we summarize the RG transformations and the exact recursion relations for the partition functions. The two ways of handling the problem are just two different ways to look at it. In the RG case, we start from a large lattice and remove short scale fluctuations by renormalizing the parameters, effectively reducing the size of the lattice. In contrast to this idea of thinning out the degrees of freedom, in the second method the lattice is built generation by generation so that one may study the behavior of any quantity of interest as a function of the length of the polymers. This is useful in studying phase transitions because finite size scaling can then be used to explore the nature of the transition.

We introduce the Boltzmann factors

$$y = \exp(\beta\epsilon) \quad \text{and} \quad w = \exp(\beta\epsilon_{123}), \tag{3}$$

where $\beta = 1/k_B T$, k_B being the Boltzmann constant and T the temperature. The RG transformations of the two-chain and the three-chain Boltzmann factors are given by

$$y' = \frac{(b-1) + y^2}{b}, \tag{4}$$

$$w' = \frac{(b-1)(b-2) + 3(b-1)y^2 + y^6 w^2}{b^2 y'^3}, \tag{5}$$

where the primed variables y' and w' on the left-hand side represent the renormalized values of the Boltzmann factors. For details see Appendix A. These recursion relations show that the three-body term is generated even though we start with $\epsilon_{123} = 0$, i.e., $w = 1$. As expected the three-chain interaction does not affect (i.e., renormalize) the two-chain interaction.

For a given y and w, the flows from successive use of Eqs. (4) and (5) would give us the phases and the nature of the transitions. One needs the fixed points for this analysis. For the two-chain system, the fixed points of y are (i) $y^* = 1$, a stable infinite temperature fixed point representing an unbound state, and (ii) $y^* = (b-1)$, an unstable fixed point representing the two-chain melting or critical point. In addition, (iii) $y^* = \infty$ (zero temperature, representing a bound duplex state) is an obvious stable fixed point, which does

not come from the RG relation but from the RG flow. For a pure three-chain interaction ($y = 1$) the fixed points of w correspond to (i) 1, infinite temperature, (ii) ($b^2 - 1$), an unstable, three-chain critical point, and (iii) ∞ (zero temperature), a stable fixed point, which comes from the RG flow. The two-chain melting is critical with a diverging length scale with exponent [19]

$$\nu = \frac{\ln \lambda}{\ln \left(\frac{dy'}{dy} \big|_{y \to y_c} \right)} \tag{6}$$

and the specific heat exponent

$$\alpha = 2 - \nu. \tag{7}$$

At the two-chain critical point $y_c = b - 1$, the fixed points of w are found to be

$$w_\pm = \frac{b^2 \pm \sqrt{4 - 24b + 32b^2 - 12b^3 + b^4}}{2(b-1)^3}. \tag{8}$$

For $b = 4$, $w_\pm = \frac{8}{27} \pm i\frac{\sqrt{23}}{27}$ are complex numbers. In the range $2.303 < b < 8.596$ no real roots are found from the three-chain RG relation [Eq. (5)] for $y = y_c$. These complex roots lead to a limit cycle behavior, which is intimately related to the Efimov effect (see Appendix C).

B. Exact recursion relations

With the trace over all configurations the nth generation partition functions for single- (C_n), double- (Z_n), and triple- (Q_n) chain systems obey the recursion relations

$$C_n = bC_{n-1}^2, \tag{9}$$

$$Z_n = b(b-1)C_{n-1}^4 + bZ_{n-1}^2, \tag{10}$$

$$Q_n = b(b-1)(b-2)C_{n-1}^6 \\ + 3b(b-1)C_{n-1}^2 Z_{n-1}^2 + bQ_{n-1}^2. \tag{11}$$

The initial conditions are taken as

$$C_0 = 1, \quad Z_0 = y, \quad Q_0 = y^3 w. \tag{12}$$

The average energy and the specific heat are defined as

$$E_n = \frac{\partial \ln Q_n}{\partial x} \quad \text{and} \quad C_n = \frac{\partial E_n}{\partial x}, \tag{13}$$

where x is the appropriate variable (y or w as the case may be). Although these definitions are different from the actual definitions, the proportionality factors are not crucial here.

For given y and w, Eqs. (9)–(11) give the partition functions for different L_n. The average energy and the specific heat can be determined for different L_n by writing down the recursion relations for derivatives of Eqs. (9)–(11).

C. Zeros of the partition functions Z_n and Q_n

If we take $w = 1$, i.e., no three-body interaction, then the partition functions are polynomials in y. In general, Z_n is a polynomial in y of order L_n while Q_n is a multinomial in y and w. These partition functions are then completely described by the zeros which are necessarily complex. A phase transition is signaled by a real limit point of the zeros. However, the rapid growth of the order of the polynomials makes it difficult to

implement this program directly. A different representation is used to get the zeros [27].

By using the RG transformations of y and w, the recursion relations from Eqs. (9)–(11) can be reduced exactly to the forms

$$Z_n(y) = b^{L_n} Z_{n-1}(y'), \tag{14}$$

$$Q_n(y,w) = (b^{L_n})^{3/2} Q_{n-1}(y',w'), \tag{15}$$

with y' and w' given by Eqs. (4) and (5). These relations can be verified by direct substitution and, if necessary, by the method of induction.

Since the zeros determine a polynomial completely, the two-chain partition functions can be written as

$$Z_n(y) = b^{L_n - 1} \prod_{l=1}^{L_n} (y - q_l), \tag{16}$$

$$Z_{n-1}(y) = b^{L_{n-1} - 1} \prod_{j=1}^{L_{n-1}} (y - \tilde{q}_j), \tag{17}$$

where the q_l's and $\tilde{q}_j$'s are the zeros of the partition functions $Z_n(y)$ and $Z_{n-1}(y)$, respectively. These zeros appear in complex-conjugate pairs. With the substitution of Eqs. (16) and (17), Eq. (14) becomes

$$b^{L_n - 1} \prod_{l=1}^{L_n} (y - q_l) = b^{L_n} b^{L_{n-1} - 1} \prod_{j=1}^{L_{n-1}} (y' - \tilde{q}_j). \tag{18}$$

Then the use of Eq. (4), the relation between y' and y, gives two roots from each factor on the right-hand side, so that the q_l's are the solutions of

$$\frac{(b-1) + y^2}{b} = \tilde{q}_j, \tag{19}$$

i.e.,

$$q = \pm\sqrt{b\tilde{q}_j - (b-1)}. \tag{20}$$

The subscript of q is omitted. This clearly shows that if we know the 2^{n-1} zeros $\tilde{q}_j$ of $Z_{n-1}(y)$, we will be able to know the 2^n zeros q_l of $Z_n(y)$. One may start with the roots of Z_1 and generate successively the roots of each generation, by just solving a quadratic equation.

Instead of generating all the roots, a random generation is more easily implementable. With an initial value y_0 chosen randomly from the two roots of Z_1, the new roots are determined by Eq. (20). If one of them is chosen at random and substituted as $\tilde{q}_j$, the roots for the next generation can be found. Thus, after the nth iteration, the set obtained is basically the zeros in the complex y plane. These roots are nothing but the zeros of the partition function found from different sizes of the lattice, which in this problem would be equivalent to different lengths of polymers. The zeros quickly converge and as $n \to \infty$ we look for the limit point on the real axis. Apart from that, the distribution in the complex y plane itself is of interest. This method has been generalized for the three-chain system.
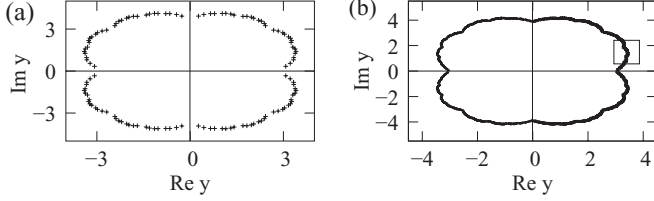
FIG. 3. Plot of zeros of $Z_n(y)$ in the complex y plane for $b = 4$ from (a) the exact recursion relation for $n = 6$ and (b) the RG relation. The closest point to the Re(y) axis approaches $y_c = 3$, the two-chain melting point in the limit $n \to \infty$, the unstable fixed point of Eq. (4). The selected region shown by a box is zoomed in Fig. 4(a).

IV. BEHAVIOR OF ZEROS: TWO-CHAIN AND THREE-CHAIN SYSTEMS

A. Two-chain system: $b = 4$

For different branching factors, fractal-like structures are obtained from the zeros of the partition functions of the two- and the three-chain systems. We considered only $b = 4$ as a representative of the range where there is no real fixed point along the two-chain critical line.

For $b = 4$ the structure shown in Fig. 3(a) is obtained in the complex y plane from the exact recursion relation Eq. (14). Exact solutions are possible only up to the $n = 6$ generation because of computational hardware limitations. This is insufficient, as the thermodynamic limit ($n \to \infty$) is needed to observe a phase transition. Finding zeros at random from the RG relations [Eqs. (4) and (5)] overcomes such difficulties and hence large lengths can be reached. The zeros obtained from Eq. (19) give the fractal-like structure shown in Fig. 3(b). The accessed zero nearest to the real axis approaches the two-chain transition point $y_c = 3$ for large n.

Apart from the limit point, the distribution of the zeros in the complex y plane is also nontrivial. The first feature to note is that the zeros do not seem to lie on a smooth differentiable curve. A zoomed picture of a small cross section of the structure for the two-chain system [from Fig. 3(b)] is shown in Fig. 4(a). Further, the selected regions have been zoomed successively and are shown in Figs. 4(b) and 4(c). The self-similarity of the structure is visible. This is an indication of the fractal nature of the distribution. Further analysis required for a quantitative description is not done here.

These fractal-like structures obtained above are nothing but the separatrices of the set of RG flows in the complex plane to the appropriate stable fixed points. These separatrices for iterations of any function in the complex plane are known as the Julia set (see Appendix B). The sets are obtained after

an infinite number of iterations of a recursive formula by identifying the points that do not flow to the stable fixed points. Our method of finding the zeros by using the RG relations is in fact equivalent to an inverse iteration method, which is more efficient in producing such structures.

In Fig. 5(a) the RG flows are shown in the complex y plane for a two-chain system. The dotted line (red curve) shows the flow towards the stable fixed point $y = 1$, i.e., the high temperature region, when we start with a value from the inner region of the fractal-like structure. On the other hand, a point from the outskirts of the line of zeros flows to the stable fixed point $y = \infty$, which is the bound state with zero temperature. The critical point, being an unstable fixed point, does not actually belong to the set but, as discussed, is a limit point—in a sense a boundary of the set.

The second feature to note is the 3-like shape near the real-axis limit point. It is not arbitrary. The angle at the limit point in the complex plane is related to the specific heat exponent by [28]

$$\tan(\phi\nu) = -\tan(\pi\alpha) + \frac{A_-}{A_+}\csc(\pi\alpha), \qquad (21)$$

where ϕ is the angle between the tangent of zeros at the limit point and the real axis of y, and $A_\pm$ are the amplitudes of the specific heat on the low and the high y side of the transition. Just like the exponents, A_-/A_+ is a universal number for a universality class of transition. For the two-chain problem, we know that $A_-/A_+ \to \infty$ as $A_+ = 0$. Therefore the angle ϕ is given by

$$\phi = \frac{\pi}{2\nu}. \qquad (22)$$

FIG. 5. (Color online) (a) Plot of zeros of $Z_n(y)$ in the complex y plane. Two types of RG flow are shown. The dotted red curve starts from a point of the inner region and flows to $y = 1$. The dashed blue curve starts from a point of the outer region and flows to ∞. (b) The triangles are the zeros and approach the limit point $y_c = 3$ at large n. The solid red line, given by Eq. (23), makes an angle ϕ with the real axis with ν of Eq. (6) and $c = y_c$.
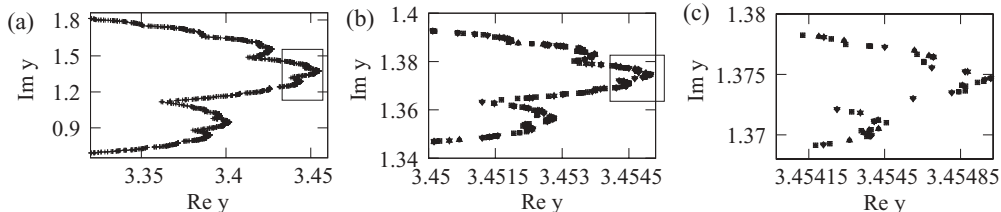

FIG. 4. Zeros of $Z_n(y)$: The inner rectangular box is zoomed successively. A self-similar structure becomes apparent. Note that the zeros are known with high accuracy.
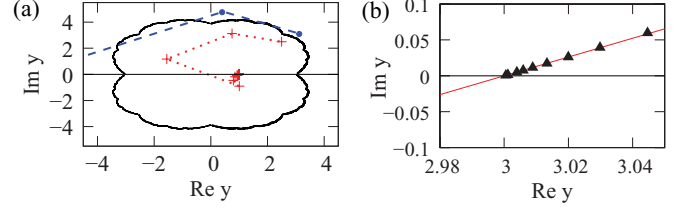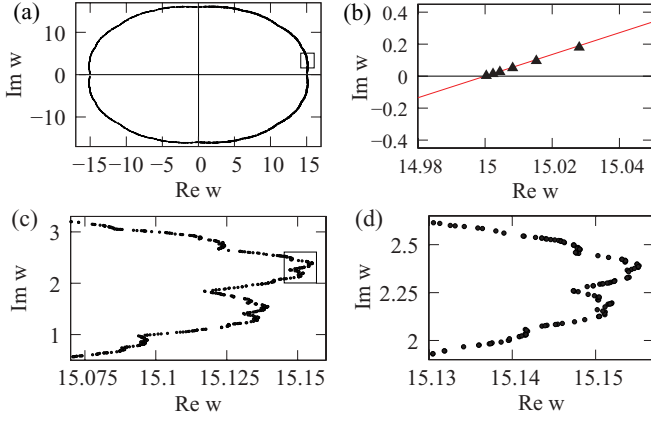
FIG. 6. (Color online) (a) Plot of the zeros of $Q_n(1,w)$ in the complex w plane for $b = 4$. The closest point to the real axis approaches $w_c = 15$ for large n. There is self-similarity in the distribution of zeros. (b) The triangles are the zeros. The solid red line given by Eq. (23) passes through them with ν of Eq. (28) and $c = w_c$. (c) and (d) The inner rectangular box [from (a)] is zoomed successively.

The zeros obtained by the successive iterations of the one close to the real axis are shown in Fig. 5(b) by the triangles. They approach the real axis in a linear fashion with an angle ϕ, given by the straight line

$$\text{Im } z = (\text{Re } z - c)\tan\frac{\pi}{2\nu} \tag{23}$$

in the generic complex z plane with ν from Eq. (6). Here c represents the limit point of the zeros on the real axis. The zeros occur in complex-conjugate pairs. Therefore if we take the mirror image of the distribution of zeros about the real axis in Fig. 5(b), the beak of the 3-like shape can be obtained.

B. Three-chain system: $b = 4$

We have calculated the zeros of $Q_n(1,w)$ for a three-chain system with a pure three-chain interaction. By considering $y = 1$ in Eq. (5), we get

$$w' = \frac{(b^2 - 1) + w^2}{b^2}. \tag{24}$$

The zeros come from the equation

$$q_l = \pm\sqrt{b^2\tilde{q}_j - (b^2 - 1)}, $$

where the q_l's and $\tilde{q}_j$'s are the zeros of $Q_n(1,w)$ and $Q_{n-1}(1,w)$, respectively. The distribution of zeros is the Julia set which has a fractal-like structure shown in Figs. 6(a), 6(c), and 6(d). By choosing the zero near to the limit point w_c, the nature of the distribution can be determined, as shown in Fig. 6(b) by the straight line given by Eq. (23) with ν of Eq. (28) and $c = w_c$.

C. Efimov DNA: $b = 4$

The idea is to show the Efimov transition point of DNA by finding the limit point of zeros on the real y axis. Although we consider $w = 1$, the effective three-chain interaction develops by renormalization. As a result the zeros found from Eqs. (9)–(11) seem to pinch the $\text{Re}(y)$ axis at a point where no pair of chains is bound. The exact solutions are shown in Fig. 7(a) for $n = 6$. On a finer scale the zeros are shown in Fig. 7(b). For such small lattices the limit point is not accessible; hence an extrapolation scheme may be used. The zeros nearest to the $\text{Re}(y)$ axis, obtained in different generations ($n = 2, \ldots, 6$) are shown in Fig. 7(c) by black dots. A straight line nicely fits these zeros and is shown by the solid red curve.

The straight line intersects the real axis at $y = 2.321$. This value is the large n extrapolation and can be taken as an estimate of the Efimov transition. We may compare this extrapolated value with the previous RG-based estimate of $y_E = 2.324\,02$. Finding the zeros for the two-chain system is easier than for the three-chain system. Since the three-chain equation holds both the variables y and w, finding zeros from the three-chain RG relation is tantamount to generating the full relation for Q_n. This is because one needs to keep w at all the intermediate values of n and then, at the desired value of n, w is to be set to 1. One sees the difficulty of the Efimov physics even though $w = 1$. It is tempting to simplify the recursion relation at the cost of some approximation. We set $w = w' = 1$ to get a renormalized y' that describes the three-chain system. Such a relation follows from Eq. (5), as

$$y'^3 = \frac{(b - 1)(b - 2) + 3(b - 1)y^2 + y^6}{b^2}. \tag{25}$$

The zeros obtained from Eq. (25) spread out in a "Milky Way" over a region in the complex plane of y. The spread makes it difficult to make an estimate of the real-axis limit point, but one may use the width to put a bound on the Efimov transition point [see Fig. 7(c)].
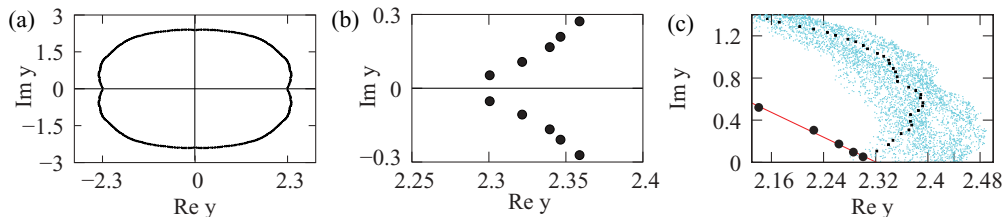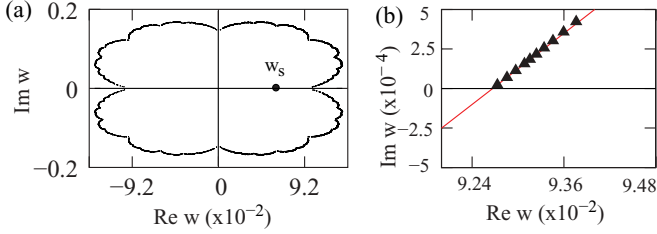

FIG. 7. (Color online) Plot of zeros in the complex y plane for $b = 4$. (a) Zeros of $Q_n(y,1)$, when $n = 6$, (b) a finer scale of (a) near the real axis, and (c) combined plot of zeros. The bigger black circles are the zeros closest to the real axis (i.e., with smallest imaginary part) obtained from $Q_n(y,1)$ for $n = 2, \ldots, 6$ and the solid (red) straight line is a fit to these. The "Milky-Way"-like region shows the distribution of zeros from Eq. (25) on which we superpose the positive quadrant of (a) shown by the small black dots.

FIG. 8. (Color online) (a) Zeros of $Q_n(y_c,w)$ in the complex w plane for $b = 9$. The stable fixed point $w = w_s$ is shown by a black circle. (b) The solid red line is given by Eq. (23) and passes through the zeros shown by the triangles, with ν from Eq. (29) and $c = w_E$.

D. Efimov DNA at $y_c = b - 1$: $b = 9$

A study along the critical threshold of the two-chain melting is quite interesting. No real fixed point for w exists for Eq. (5) when b is in the range $2.303 \leqslant b \leqslant 8.596$ along the $y = y_c$ line. For $y = y_c$, the single parameter RG relation is

$$w' = \frac{(b-2) + 3(b-1)^2 + (b-1)^5 w^2}{b^2(b-1)^2}. \qquad (26)$$

The two fixed points for this case are given by Eq. (8). For $b = 9$, these are

$$w = w_s = 0.065\,534\,7\ldots \text{ (stable)}, \qquad (27a)$$

$$w = w_E = 0.092\,668\,4\ldots \text{ (unstable)}. \qquad (27b)$$

The unstable fixed point, as the phase transition point, determines the limit point of the zeros of the partition function on the real axis. Hence it can be predicted that at the two-chain melting point, by tuning w, a transition occurs at $w = w_E$, from the Efimov DNA to the critical state of polymer pairs. Figure 8(a) shows the distribution of zeros of $Q_n(y_c,w)$ in the complex w plane. The set of these zeros is a Julia set, separating the flows to the stable fixed points. The stable fixed point in the inner region of the set is given by Eq. (27a). The zeros near the real axis approach $w = w_E$ linearly, following Eq. (23) with $c = w_E$ and ν of Eq. (29) as shown in Fig. 8(b). A detailed discussion is given in the next section.

V. EFIMOV DNA: RG FLOW AND NUMERICAL EVIDENCE

To explore the robustness of the Efimov effect, we now include a three-chain repulsive interaction along with the pairwise attractive one. The three-chain interaction is attractive when $w > 1$ and repulsive for $0 \leqslant w < 1$. For $w = 0$, representing the hard core three-chain repulsive interaction, three chains can never be on the same bond in this model.

A. $b = 4$

For $b = 4$ the RG phase diagram is shown in Fig. 9(a). The solid red line is the separatrix connecting the pure three-chain transition point $(1, w_c)$ to an Efimov transition point for $w = 0$. Each point on the solid line represents an Efimov transition point. In other words keeping w fixed, by changing y, we can see a melting of a loosely bound Efimov DNA with no pairwise binding.
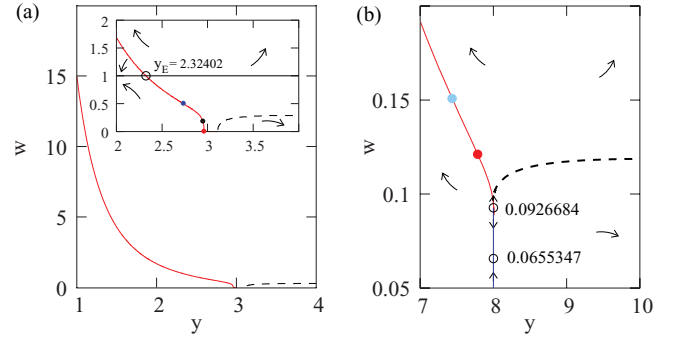

FIG. 9. (Color online) RG phase diagram in the y-w plane. The arrows are to show the flow of the renormalized parameter schematically. (a) For $b = 4$. The solid red curve and the dashed curve represent the separatrices, where w flows to two different fixed points on either side of the separatrix. The zoomed area near $y_c = 3$ is shown in the inset. For $w = 1$, $y_E = 2.324\,02$ is the Efimov DNA transition point. The filled circles are the Efimov transition points for $w = 0.5$, $w = 0.2$, and $w = 0$ respectively, obtained from Fig. 10(a). (b) For $b = 9$. Along $y_c = 8$, there are two real fixed points given by Eq. (27a). The solid (red) and dashed lines are the separatrices. The filled circles are the Efimov transition points for $w = 0.15$ and $w = 0.12$, respectively, obtained from Fig. 10(b).

The region enclosed between this separatrix (solid red line) and the $y_c = 3$ line is the Efimov region and (y,w) flows to $(1,\infty)$. Below the solid red line is the high temperature zone of denatured DNA, where RG flows are to $(1,1)$. The region to the right of the $y_c = 3$ line is the two-chain bound state. The area below the dashed curve, where the RG flow takes w to zero when two-chain pairs are strongly bound, represents a different state where one finds a three-chain bound state but with no three-chain contact. The dashed line is then a crossover line. It remains to be seen if under some conditions this crossover line becomes a true phase transition line.

B. $b = 9$, $y_c = b - 1$

The RG phase diagram is shown in Fig. 9(b) for $b = 9$. In the diagram two separatrices (the solid red line and the dashed line) meet at an unstable fixed point. The two fixed points $w = w_s$ and $w = w_E$ are shown in Fig. 9(b). The presence of any unstable fixed point reflects a continuous transition along the two-chain critical line. Hence we can say that by tuning the three-chain repulsive interaction parameter or temperature in the repulsive zone a transition can be induced in the Efimov DNA at the critical threshold of duplex binding. The transition is from the Efimov state to the critical state of pairs dominated by the three-chain repulsion. The Efimov region is now restricted by a separatrix connecting the two unstable fixed points $(1, w_c)$ and (y_c, w_E) and the critical line $y_c = b - 1$.

On the critical line at both the fixed points $w = w_s$ and $w = w_E$, y is a relevant variable (unstable in the y direction). But y does not couple to w in the RG equation [Eq. (4)]. The melting for $w < w_E$ would be similar to the pure two-chain melting described by Eqs. (6) and (7). In the y-w plane, (y_c, w_E) is a multicritical point where the line of first-order transitions goes over to a line of critical points.
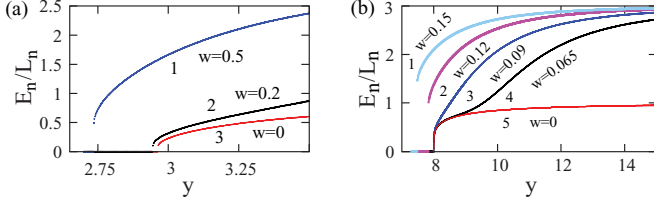
FIG. 10. (Color online) The three-chain average energy per monomer with y from direct computation. (a) For $b = 4$, the average energy curves (marked 1, 2, and 3) with the fixed values $w = 0.5$, $w = 0.2$, and $w = 0$ show first-order transitions. (b) For $b = 9$, the average energy curves (marked 1 and 2) with the fixed values $w = 0.15$ and $w = 0.12$ show first-order transitions. Curves (marked 3, 4, and 5) with the constant values $w = 0.09$, $w = 0.065$, and $w = 0$ show a continuous transition at $y_c = 8$.

C. Data collapse

We now provide numerical evidence for the above RG-based inferences. Exact numerical calculations of the average energy and the specific heat are done by iterating the partition functions and their higher derivatives for lattices of various sizes for different fixed values of w. Figure 10(a) for $b = 4$ shows that at $w = 0.5$, $w = 0.2$, and $w = 0$, there are first-order transitions. The transition points estimated from the point of discontinuity are shown by the filled circles in Fig. 9(a). They are on the separatrix and are the Efimov transition points for the corresponding values of w.

The energy curves in Fig. 10(b) for $b = 9$ with $w = 0.15$ and $w = 0.12$ show first-order transitions. These transition points are shown by the filled circles in Fig. 9(b). In contrast, the energy curves (marked 3, 4, and 5) show continuous transitions for $w = 0.09$, $w = 0.065$, and $w = 0$, respectively, at $y_c = 8$. This is consistent with the RG prediction of Fig. 9(b).

The energy and the specific heat curves are shown in Figs. 11(a) and 11(b) for $b = 9$, $y = 1$ and in Figs. 12(a) and 12(b) for $b = 9$, $y_c = b - 1$. Also the corresponding finite size scaling is shown in Figs. 11(c) and 11(d) for $b = 9$, $y = 1$ and in Figs. 12(c) and 12(d) for $b = 9$, $y_c = b - 1$. The finite
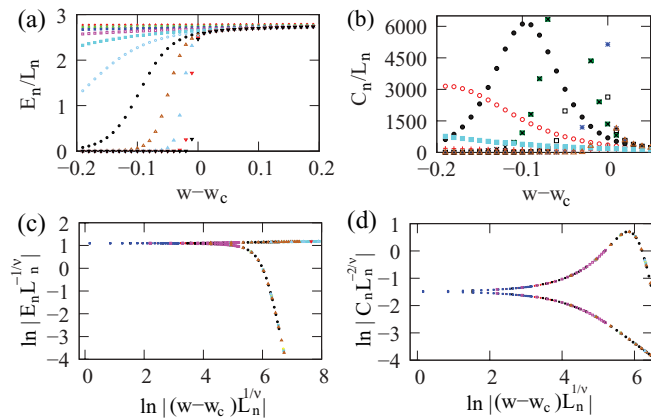

FIG. 11. (Color online) For $b = 4$. (a) The three-chain average energy per monomer versus the corresponding Boltzmann factor for chain length up to 2^{26} when $y = 1$. The average energy shows a continuous transition at $w = w_c$. (b) The three-chain specific heat (C_n) per monomer with the corresponding Boltzmann factor. (c) Data collapse of energy. (d) Data collapse of specific heat.
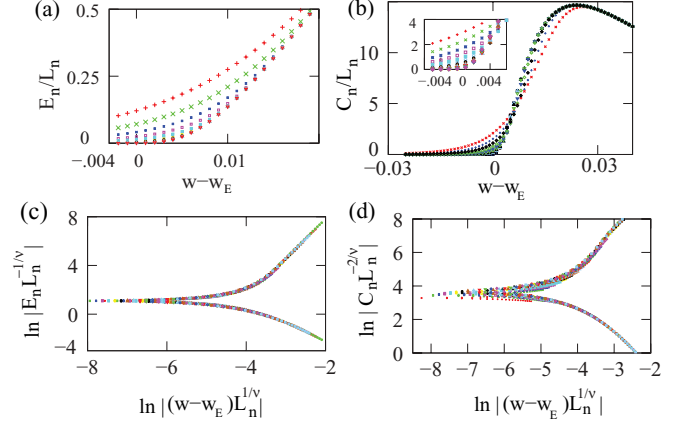

FIG. 12. (Color online) For $b = 9$. (a) The three-chain average energy per monomer versus the corresponding Boltzmann factor for chain length up to 2^{26} when $y_c = b - 1$. The average energy shows a continuous transition at $w = w_E$. (b) The three-chain specific heat (C_n) per monomer with the corresponding Boltzmann factor. The length dependence is shown in the inset. (c) Data collapse of energy. (d) Data collapse of specific heat.

size scaling behavior of different thermodynamic quantities is described by the length scale exponents. In analogy with Eq. (6), the exponents to describe the three-chain transition for $y = 1$ and $y_c = b - 1$ at appropriate critical points are given by

$$\nu = \frac{\ln 2}{\ln \frac{2(b^2 - 1)}{b^2}}, \tag{28}$$

$$\nu = \frac{\ln 2}{\ln \left(\frac{\partial w'}{\partial w} \Big|_{\substack{y_c = b - 1 \\ w \to w_E}} \right)}. \tag{29}$$

Around a critical point one should see a finite size scaling. Therefore the average energy and the specific heat obeying the finite size scaling can be written in the forms

$$E \sim L^{1/\nu} f(L^{1/\nu} |w - w^*|), \tag{30}$$

$$C \sim L^{2/\nu} f(L^{1/\nu} |w - w^*|), \tag{31}$$

with appropriate ν and w^*.

In Figs. 11(c) and 11(d) we see that the average energy and the specific heat scale as $E_n L_n^{-1/\nu}$ and $C_n L_n^{-2/\nu}$, respectively, when plotted versus $|(w - w^*)| L_n^{1/\nu}$ with the ν of Eq. (28) and $w^* = w_c$ for $y = 1$, all the data collapse onto a single curve for different lengths of polymers, where $n = 6, 7, \dots, 26$.

Figures 12(c) and 12(d) show similar plots for the critical line ($y_c = b - 1$) with ν of Eq. (29) and $w^* = w_E$. Since the specific heat diverges with increasing length, data collapse is good for the case $y = 1$. The data collapse for the case $y_c = b - 1$ is not so good due to a smoother behavior of the specific heat at the critical point. These establish the weak criticality at $w = w_E$.

VI. SUMMARY

To summarize, the RG relations and exact recursion relations are used to study the three-chain system on a diamond

hierarchical lattice. Our emphasis is on the Efimov-like state exhibited by the three-chain system at or beyond the two-chain melting, where no two chains are bound, and the nature of the transitions. Fractal-like structures are obtained for the zeros of the partition functions. These zeros, when they pinch the real axis, determine the phase transition points. We find that all the transition points obtained from RG flows, are in good agreement with the zeros of the partition function on the real axis. The Efimov transition point thus found strengthens the prediction of Efimov-like phenomena for the three-chain system. We have shown that the Efimov effect is exhibited by a three-chain system even if there is a repulsive three-chain interaction. A transition can be induced in higher dimensions from the Efimov state to the three-chain critical repulsive state at the melting of duplex DNA. The transition to this three-chain critical repulsive state is continuous and obeys a finite size scaling law with exponents obtained from the RG. In the (y,w) phase diagram, (y_c, w_E) is a multicritical point.

Although the model studied in this paper is simplistic, mainly to get exact results, still the denaturation transition induced by bubble formation accompanied by diverging length scales is the generic scenario for more realistic polymeric models. The qualitative picture is therefore expected to be valid for those models too. We await experimental evidence for the existence of the Efimov DNA or the Efimov transition. Again, the existence of such a state remains a challenge for molecular dynamics and Monte Carlo simulations.

APPENDIX A: RG RELATIONS

The configurations of the two-chain system on a motif of a hierarchical lattice can be classified as two independent chains or inherently two-chain configurations as shown in Fig. 2(c). By summing over all configurations the partition functions for $n = 0$ and $n = 1$ generation lattices for general b can be written as [9,19]

$$Z_0(y) = y, \tag{A1}$$

$$Z_1(y) = b(b-1) + by^2. \tag{A2}$$

In RG decimation, $2b$ bonds of the $n = 1$ generation are replaced by a single bond at the $n = 0$ generation. Then RG demands

$$Z_0(y') \propto Z_1(y), \tag{A3}$$

where y' is the renormalized Boltzmann factor. With the free chain boundary conditions (i.e., $y = 1$ implies $y' = 1$), the proportionality constant of Eq. (A3) can be determined. The RG transformation for the two-chain Boltzmann factor then becomes

$$y' = \frac{b(b-1) + by^2}{b^2}. \tag{A4}$$

The RG relation for the three-chain case can also be written in the same spirit as in the two-chain case. The free chain

condition is that $y = w = 1$ implies $y' = w' = 1$. It is also to be noted that when three chains share the same bond the contribution is $y^3 w$. The RG transformation for w is then

$$y'^3 w' = \frac{b(b-1)(b-2) + 3b(b-1)y^2 + by^6 w^2}{b^3}, \tag{A5}$$

where w' is the renormalized value of w.

APPENDIX B: JULIA SET

The standard definition of a Julia set is the set of points on the complex plane which flow to a fixed point (no divergence) after a function, e.g.,

$$z_n = z_{n-1}^2 + c, \tag{B1}$$

is repeatedly applied, where c is any arbitrary constant and could be real or complex. Let us choose $c = 0$. The fixed point solutions for $c = 0$ are $z = 0, 1, \infty$, where $z = 1$ is the unstable fixed point. Here, for $n \to \infty$, $z_{n+1} \to 0$ when we start with $|z_0| < 1$ and $z_{n+1} \to \infty$ when we start with $|z_0| > 1$. Therefore the unit circle $|z| = 1$ is the boundary between the two stable fixed points $z = 0, \infty$. The unstable point lies on this boundary.

APPENDIX C: LIMIT CYCLE

For two successive generations Eqs. (5) will be

$$w_n - w_{n+1} = f(w_{n+1}) - w_{n+1}. \tag{C1}$$

But if the continuum limit is taken, Eq. (C1) can be written as

$$l\frac{dw}{dl} = -(w - w_+)(w - w_-) \tag{C2}$$

at the critical line $y_c = b - 1$, where $l = \ln L$ and $L = 2^n$. For complex $w_\pm = \alpha \pm i\beta$, the solution of Eq. (C2) is then

$$w = \alpha - \beta \tan \beta(\ln l + \theta), \tag{C3}$$

where θ is the integration constant. The above equation reflects the periodicity of w in $\ln l$ with the property

$$w(l) = w(l\lambda) \quad \text{where } \ln \lambda = \frac{\pi}{\beta}. \tag{C4}$$

Here as l increases w approaches $\pm\infty$. This behavior can be mapped into a limit cycle in the complex plane with a phase factor defined by the equation

$$e^{i\phi} = \frac{w - w_+}{w - w_-}. \tag{C5}$$

With the help of Eq. (C2) and its derivative, ϕ will be

$$\phi = \frac{\beta}{\alpha} \ln l + \phi_0, \tag{C6}$$

where ϕ_0 is the integration constant.

Our model on the hierarchical lattice is a discrete model. Certainly a limit cycle is obtainable from the RG relations in the continuum limit, but it is not straightforward to do so in the discrete case.

[1] G. Felsenfeld, D. R. Davies, and A. Rich, J. Am. Chem. Soc. **79**, 2023 (1957).

[2] H. E. Moser and P. B. Dervan, Science **238**, 645 (1987).

[3] T. Le Doan *et al.*, Nucleic Acids Res. **15**, 7749 (1987).

[4] A. Jain *et al.*, Biochimie **90**, 1117 (2008); M. Duca *et al.*, Nucleic Acids Res. **36**, 5123 (2008).

[5] Michael M. Seidman and Peter M. Glazer, J. Clin. Invest. **112**(4), 487 (2003).

[6] R. W. Roberts and D. M. Crothers, Science **258**, 1463 (1992).

[7] P. E. Nielsen, Annu. Rev. Biophys. Biomol. Struct. **24**, 167 (1995).

[8] L. Betts *et al.*, Science **270**, 1838 (1995).

[9] Jaya Maji, S. M. Bhattacharjee, F. Seno, and A. Trovato, New J. Phys. **12**, 083057 (2010).

[10] V. Efimov, Phys. Lett. B **33**, 563 (1970).

[11] V. N. Efimov, Yad. Fiz. **12**, 1080 (1970) [Sov. J. Nucl. Phys. **12**, 589 (1971)].

[12] V. Efimov, Sov. J. Nucl. Phys. **29**, 546 (1979).

[13] A. C. Fonseca, E. F. Redish, and P. E. Shanley, Nucl. Phys. A **320**, 273 (1979).

[14] M. Zaccanti *et al.*, Nat. Phys. **5**, 586 (2009).

[15] T. Kraemer *et al.*, Nature (London) **440**, 315 (2006).

[16] D. V. Fedorov, A. S. Jensen, and K. Riisager, Phys. Rev. Lett. **73**, 2817 (1994).

[17] E. Braaten and H.-W. Hammer, Phys. Rep. **428**, 259 (2006).

[18] Efimov DNA is not like Borromean rings. Borromean rings remain linked even in the denatured state of DNA because of their closed form. On the other hand the closed form of DNA is not a necessity for Efimov DNA.

[19] S. Mukherji and S. M. Bhattacharjee, Phys. Rev. E **52**, 1930 (1995).

[20] M. Kaufman and R. B. Griffiths, Phys. Rev. B **24**, 496 (1981).

[21] T. A. S. Haddad and S. R. Salinas, Physica A **306**, 98 (2002); T. A. S. Haddad, R. F. S. Andrade, and S. R. Salinas, J. Phys. A **37**, 1499 (2004).

[22] M. Hinczewski and A. N. Berker, Phys. Rev. E **73**, 066126 (2006).

[23] C. N. Yang and T. D. Lee, Phys. Rev. **87**, 404 (1952).

[24] T. D. Lee and C. N. Yang, Phys. Rev. **87**, 410 (1952).

[25] M. E. Fisher, *Lectures in Theoretical Physics*, Vol. 7 (University of Colorado Press, Boulder, 1965).

[26] G. Julia, J. Math. Pures Appl. **4**, 47 (1918).

[27] B. Derrida, L. De Seze, and C. Itzykson, J. Stat. Phys. **33**, 559 (1983).

[28] C. Itzykson, R. B. Pearson, and J. B. Zuber, Nucl. Phys. B **220**, 415 (1983).